

Role of Amphiphilic Dopants on the Shape and Properties of Electrically Conducting Polyaniline-Clay Nanocomposite

Viswan L. Reena,¹ Janardhanan D. Sudha,² Chorappan Pavithran¹

¹Materials and Minerals Division, CSIR, Thiruvananthapuram 695019, India

²Chemical Sciences and Technology Division, CSIR, Thiruvananthapuram 695019, India

Received 9 December 2008; accepted 22 March 2009

DOI 10.1002/app.30525

Published online 27 May 2009 in Wiley InterScience (www.interscience.wiley.com).

ABSTRACT: The role of functionality and rigidity of the amphiphilic dopants on the morphology and electrical property of the polyaniline-clay nanocomposites (PANICNs) were studied by preparing polyaniline (PANI) and PANICNs using five structurally different amphiphilic dopants having backbone—phenyl, naphthyl, alicyclic, and alkyl groups. Effect of the size and functionality of the dopant on the extent of intercalation/exfoliation, morphology, thermal stability, and phase transitions were studied. PANICNs exhibited different morphologies such as nano/micro granules, rods, nanotubes, aggregated layers/clusters, and rice grain for PANICN-2,6-naphthalene sulphonic acid, PANICN-*para*-toluene sulphonic acid, PANICN-ste-

aric acid, PANICN-dodecyl benzene sulphonic acid, and PANICN-camphor sulphonic acid, respectively. X-ray diffraction, Fourier transform infrared, and scanning electron microscopic studies showed that the self-assembled nano/microstured aggregates were formed by the combined effect of many noncovalent interactions such as phenyl-phenyl stacking, hydrogen bonding, ion-dipole interaction, π - π stacking, and electrostatic layer-by-layer self-assembling. © 2009 Wiley Periodicals, Inc. *J Appl Polym Sci* 113: 4066–4076, 2009.

Key words: amphiphilic; conducting; nanocomposite; polyaniline; self-assembling

INTRODUCTION

Electrically conducting polyaniline-clay nanocomposites (PANICNs) comprising nanofibers and nanotubes have been received considerable research interest because of their dramatic improvement in mechanical, physical, conducting, and optoelectronic properties.^{1–9} Polyaniline (PANI) is an important conducting polymer because of its high conductivity,^{10,11} unique redox property,^{12–14} easier method of synthesis,¹⁵ and tuning of the properties via appropriate doping.¹⁶ They are prepared by different strategies for potential applications as chemical sensors, actuators, light emitting diodes, and gas separation membranes.¹⁷ Conjugated polymers encapsulated in two-dimensional layers of inorganic hosts offer fascinating strategies for designing materials with intriguing properties. The constrained environment of an inorganic host should lead to a high degree of polymer order within the host, and this may have profound effects on physicochemical properties and electrical conduction mechanisms. Generally, PANI nanofibers and nanotubes have been prepared by

chemical or electrochemical oxidation polymerization of aniline with the aid of either templates or structure-directing molecules.^{18–21} There are many routes for preparing inorganic-organic hybrid materials such as micelle media,²² template-guided,^{23,24} or in the presence of inorganic-layered materials.^{25–27}

Montmorillonite is one of the most abundant naturally occurring layered materials having high aspect ratio and surface area. In addition to that, the surface of the montmorillonite is easily amenable for modification. They contain thin layers of aluminum silicate organized themselves in a parallel fashion to form stacks with a regular van der Waal gap in between them called interlayer spacing or gallery. In the interlayer region, there exists ions like Na^+ and Ca^{2+} that can be easily replaced with the alkyl ammonium or alkylphosphonium ions.²⁸ One of the commonly used method to prepare PANICN is the intercalation of anilinium salt of dodecylsulphonic acid into the gallery of clay followed by in-situ polymerization.^{29–31} Literature shows that amphiphilic dopants comprising both hydrophobic as well as hydrophilic group can function as intercalating agents and can reduce the intergallery interaction. They can maximize the affinity between hydrophilic host (clay) and hydrophobic guest (aniline) and also serve as dopant for PANI. A variety of amphiphilic

Correspondence to: J. D. Sudha (sudhaid2001@yahoo.co.in).

dopants that belong to the families of sulphonic acids, phosphonic acids, and phosphoric acid esters are reported.^{32–34} After intercalation of the anilinium ion (An^+)⁻OR, the extrinsic initiator ammonium persulfate (APS) can enter and initiate polymerization for getting protonated PANI chain confined PANICNs. PANI increases the conductivity not only due to the carrier concentration but also due to the enhanced mobility of the charge carriers, which occurs at higher doping level. In fact, conductivity can be expressed as $\sigma = ne\mu$, where e is the electronic charge, n is the density of the charge carriers, and μ is the mobility of the charge carriers. Thus, the conductivity of the doped PANI is dominated by the density and mobility of the charge carriers. Thus, it is expected that the size and the functionality of the amphiphilic dopant can influence the extent of intercalation, electrical conduction, and also shape of the formed micro/nanostructured PANICNs. Here, we present the effect of rigidity and functionality of five structurally different amphiphilic dopants on the properties like conductivity, morphology, thermal stability, and phase transition temperature of PANIs and PANICNs.

EXPERIMENTAL

Materials

Aniline (99.5% pure, Ranbaxy chemicals Ltd., Bombay) was distilled under reduced pressure before use. APS, methyl alcohol, *para*-toluene sulphonic acid (PTSA), and stearic acid (SA) were purchased from Sd. Fine Chemicals Ltd, Bombay, India. Na^+ cloisite with cation exchange capacity of 92.6 meq/100 g and a mean chemical formula of $(\text{Na,Ca})_{0.33}(\text{Al}_{1.67}\text{Mg}_{0.33})\text{Si}_4\text{O}_{10}(\text{OH})_2.n\text{H}_2\text{O}$ was purchased from Loba Chemie, Bombay, India. Before use it was washed many times with saturated sodium chloride solution and size fractionated to obtain clay free of impurities. Dodecyl benzene sulphonic acid (DBSA) (85% in isopropanol), camphor sulphonic acid (CSA), and 2,6-naphthalene sulphonic acid (NSA) (~99.5%) purchased from Aldrich was used without further purification.

Preparation of PANI-DBSA and PANICN-DBSA

A total of 0.3 g of Na^+ cloisite in 200 mL deionised water was refluxed in a three-necked round bottomed flask by heating and stirring at 80°C for 3 hrs. An aqueous solution of 3 g of aniline (0.032 moles) containing 15.77 g (0.048 moles) DBSA was added drop wise to the clay dispersion. Heating and stirring were continued for 2 to 6 hrs. The solution was then cooled down to room temperature and pH was adjusted to 2 to 3 using 11N hydrochloric acid. APS

(0.04 mole) dissolved in 50 mL of water was then added drop wise to initiate the polymerization. Reaction was continued for 3 to 4 hrs. PANICN formed was precipitated with methanol. The product was isolated by filtration, washed with deionised water several times, finally with methanol and then dried overnight in a vacuum oven at 60°C.

Yield 77%, color and appearance: emeraldine green powder. Similar synthesis were carried out with dopants like NSA, PTSA, SA, and CSA.

Instrumentation

UV-vis absorption spectra of the PANIs and PANICNs were studied by coating thin films of the sample on a glass plate and recording the spectra using UV-vis spectrophotometer (Shimadzu model 2100) in the range of 300 to 1100 nm. Fourier transform infrared (FT-IR) measurements of PANIs and PANICNs were observed with a fully computerized Nicolet impact 400D FT-IR spectrophotometer. Polymers were dispersed in potassium bromide and compressed into pellets before recording. All spectra were corrected for the presence of moisture and carbon dioxide in the optical path. The interlayer distance of the clay layers and the formation of self-assembled structures of PANIs and PANICNs were measured using powder X-ray diffractometer (XRD; Philips X'pert Pro) with CuK_α radiation ($\lambda = 0.154$ nm) using X'celerator detector and monochromator at the diffraction beam side. Powder samples were studied using standard sample holder. Averaged 2 θ was used with the 2 θ resolution of 0.002° from 2 to 10°.

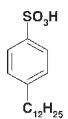
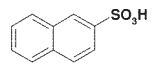
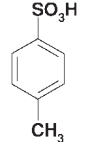

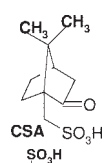
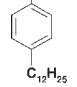
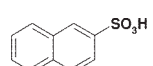
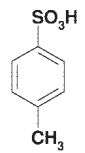

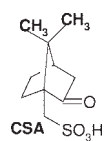
Electrical conductivity (σ_{dc}) of uniform sized pressed pellets at 30°C was measured using the standard spring-loaded pressure contact four probe method supplied by Scientific Equipment, Roorkee (India). The conductivity (σ_0) was calculated using van der Pauw relation

$$\sigma_0 = (\ln 2/\pi d)(I/V) \quad (1)$$

where d is the thickness of the pellet, I is the current in ampere, and V is the voltage in volts.

Morphological studies of PANICNs pelletized powder samples were studied using scanning electron microscope (SEM, JEOL make, model JSM 5600 LV) at 15 kV accelerating voltage. Differential scanning calorimetry (DSC) were performed using Dupont DSC 2010 attached to Thermal Analyst 2100 data solution under nitrogen atmosphere at a heating rate of 10°C/min from 30 to 200°C. Thermal stability measurements were performed at a heating rate of 10°C/min in nitrogen atmosphere using Shimadzu, DTG-60 equipment from 30 to 600°C for PANIs and 30 to 800°C for PANICNs.

TABLE I
Polymerization Characteristics of PANIs and PANICNs

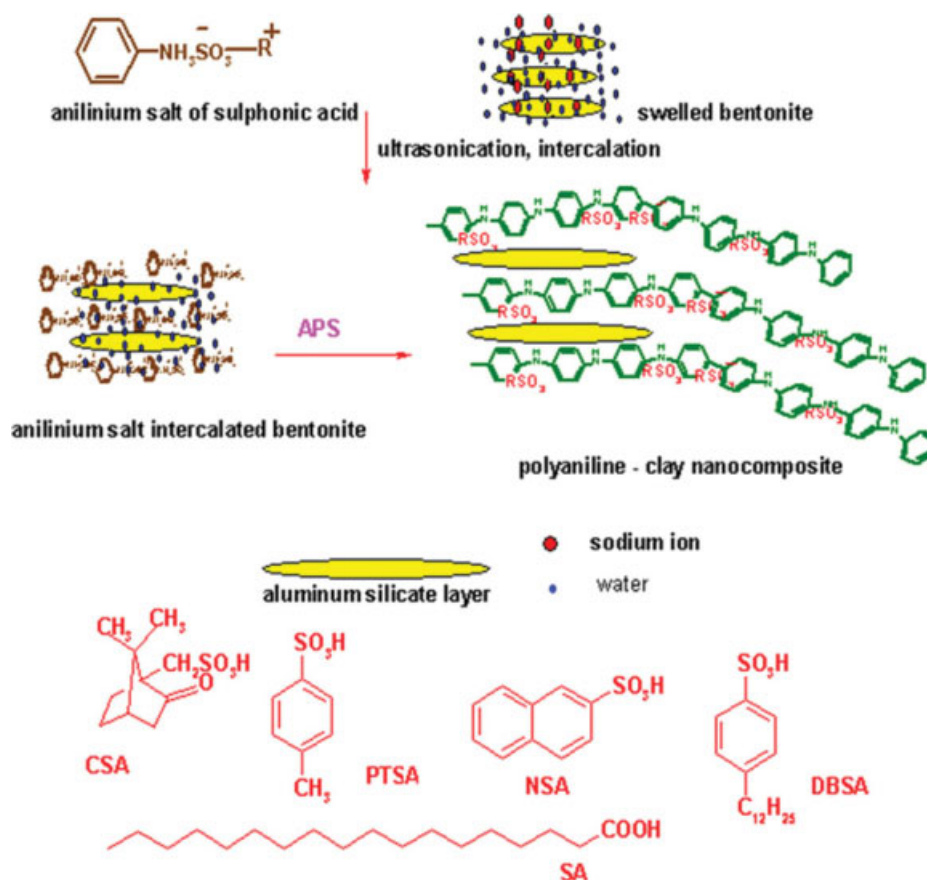
Sample	Dopant	No. moles of dopant	No. moles of aniline	Wt % of clay	% Yield	Colour and appearance
PANI-DBSA		0.012	0.008	0	60	Emeraldine green powder
PANI-NSA		0.012	0.008	0	70	Emeraldine green powder
PANI-PTSA		0.012	0.008	0	76	Emeraldine green powder
PANI-SA		0.012	0.008	0	60	Emeraldine green powder
PANI-CSA		0.012	0.008	0	76	Emeraldine green powder
PANICN-DBSA		0.048	0.032	5	77	Emeraldine green powder
PANICN-NSA		0.048	0.032	5	80	Emeraldine green powder
PANICN-PTSA		0.048	0.032	5	80	Emeraldine green powder
PANICN-SA		0.048	0.032	5	65	Emeraldine green powder
PANICN-CSA		0.048	0.032	5	77	Emeraldine green powder

RESULTS AND DISCUSSION

Preparation of PANIs and PANICNs

Nanostructured electrically conducting PANIs and PANICNs were prepared by in-situ intercalative emulsion polymerization of anilinium salts of DBSA, NSA, PTSA, SA, and CSA in aqueous dispersion of clay at 0 to 5°C using APS as oxidant initiator as per the procedure reported earlier.³⁵ Experimental details are illustrated in Table I. PANICNs prepared using dopants DBSA, NSA, PTSA, SA, and CSA are designated as PANICN-DBSA, PANICN-NSA, PAN-

ICN-PTSA, PANICN-SA, and PANICN-CSA, respectively, and the corresponding protonated PANIs without clay are indexed as PANI-DBSA, PANI-NSA, PANI-PTSA, PANI-SA, and PANI-CSA. At the beginning of polymerization, only the totally oxidized form of the PANI, the pernigraniline form is present (copper tint color). Then, polymer chain can add monomer until its oxidation stage achieves emeraldine green form.³⁶ These amphiphilic molecules act the dual role of intercalating agent cum dopant in the preparation of electrically conducting PANICNs as shown in Scheme 1. Synthesized PANIs and



Scheme 1 Preparation of polyaniline-clay nanocomposites. [Color figure can be viewed in the online issue, which is available at www.interscience.wiley.com.]

PANICNs were in the emeraldine green color indicating that they were in the doped conducting state. PANI doping consists of the protonation of the polymer imine nitrogen atoms followed by charge redistribution to give a polysemiquinone radical-type molecular structure.³⁷ Now, if another electron is removed from the already oxidized PANI, it can create another polaron or a bipolaron. As these polarons and bipolarons are mobile they can, therefore,

move along the polymer chain through the rearrangement of double and single bonds. Solubility studies of PANIs and PANICNs were performed in various solvents having different polarity. It was observed that doped PANIs were completely soluble in *m*-cresol and partially soluble in solvents like chloroform and toluene, whereas PANICNs are only partially soluble. Details of the solubility studies are given in Table II.

TABLE II
Studies on the Solubility of PANIs and PANICNs

Sample	<i>m</i> -Cresol	DMF	Chloroform	Toluene
PANI-DBSA	Completely soluble	Partially soluble	Partially soluble	Partially soluble
PANI-NSA	Completely soluble	Completely soluble	Partially soluble	Partially soluble
PANI-PTSA	Completely soluble	Completely soluble	Partially soluble	Partially soluble
PANI-SA	Completely soluble	Completely soluble	Partially soluble	Partially soluble
PANI-CSA	Completely soluble	Partially soluble	Partially soluble	Partially soluble
PANICN-DBSA	Partially soluble	Insoluble	Partially soluble	Insoluble
PANICN-NSA	Partially soluble	Partially soluble	Insoluble	Insoluble
PANICN-PTSA	Partially soluble	Partially soluble	Insoluble	Insoluble
PANICN-SA	Partially soluble	Partially soluble	Insoluble	Insoluble
PANICN-CSA	Partially soluble	Insoluble	Partially soluble	Insoluble

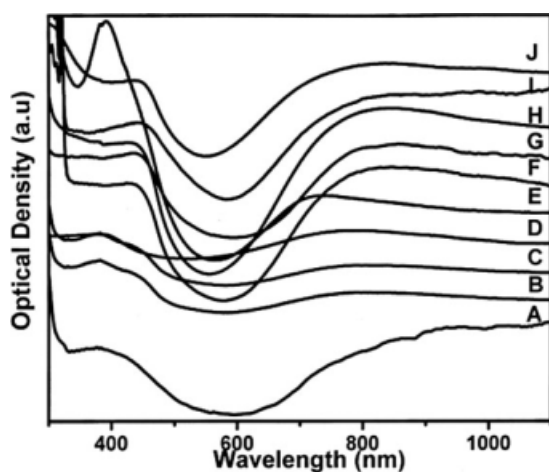


Figure 1 UV-vis spectra of (A) PANI-DBSA, (B) PANI-NSA, (C) PANI-PTSA, (D) PANI-SA, (E) PANI-CSA, (F) PANICN-DBSA, (G) PANICN-NSA, (H) PANICN-PTSA, (I) PANICN-SA, and (J) PANICN-CSA.

Structural characterization

UV-vis and FT-IR spectroscopy

Electronic structures of PANIs and PANICNs were studied by UV-vis spectral techniques. UV-vis spectroscopy is a sensitive tool for studying the nature of PANI protonation. UV-vis spectra of PANI-DBSA, PANI-NSA, PANI-PTSA, PANI-SA, PANI-CSA, PANICN-DBSA, PANICN-NSA, PANICN-PTSA, PANICN-SA, and PANICN-CSA are given in Figure 1(A–J). Except for PANI-SA, PANICN-PTSA, and PANICN-SA, the UV-vis spectra of all the PANIs and PANICNs exhibited three absorption peaks in the region (i) $\sim 300\text{--}340\text{ nm}$ ($\pi\text{--}\pi^*$ transition of benzenoid amine structure of PANI) (ii) $\sim 430\text{ nm}$ (corresponding to the transition of polaron band to π^*),³⁸ and (iii) $\sim 700\text{--}850\text{ nm}$ (π -polaron band transition).^{39,40} In the former case, the transition between π band to π^* band ($\sim 300\text{ nm}$) becomes very weak, because the energy gap between the π band and the polaron band has been eliminated,⁴¹ and hence exhibited peak only at $\sim 430\text{ nm}$ and $\sim 750\text{ nm}$. In PANICNs a red shift is observed for the peak at $\sim 700\text{ nm}$ and is observed as a broad absorption band (called free carrier tail) in the near infra red region. It is consistent with the delocalization of electrons in the polaron band promoted by an extended conformation of the PANI chains. Moreover, the twist defects between the aromatic rings intercalated between the clay layers are removed and the interaction between adjacent isolated polarons, therefore, becomes stronger and the polaron band becomes more dispersed in energy (more delocalized). These observations were further strengthened during the measurement in conductivity.

FT-IR spectral technique can be used in studying the interactions between the dopant anion and the PANI chains and also the interaction between PANI chains and clay surface. FT-IR spectra of PANIs and PANICNs are given in Figure 2(A–J). Generally, all the PANIs showed similar peaks except vibrations corresponding to the dopant anions. The characteristic bands corresponding to pristine bentonite are 1023 cm^{-1} [$\nu(\text{Si-O})$], 911 cm^{-1} [$\delta(\text{Al-OH})$] and 525 cm^{-1} [$\nu(\text{Si-O-Al})$].^{42–45} The $(\text{C=C})_{\text{str}}$ deformation of the quinoid in PANICNs shifted from 1590 to 1572 cm^{-1} and that of the benzenoid ring from 1502 to 1485 cm^{-1} , indicating the longer effective conjugation lengths.^{46–48} However, from a closer look at the spectra, it was observed that the band at 1295 cm^{-1} , assigned as the stretching vibration of C–N, is significantly shifted to 1300 to 1305 cm^{-1} in PANICNs. This frequency shift of $\nu(\text{C-N})$ observed in PANICNs are believed to be caused by the hydrogen bond interaction between PANI and the basal surface of bentonite clay (i.e., $\text{NH}\cdots\text{O}$ hydrogen bonding). The bands at 1040 and 506 cm^{-1} can be assigned due to the sulphonate anion present in PANIs and PANICNs.

X-ray diffractometer

XRD is an efficient analytical tool to probe the extent of intercalation/exfoliation and the dimension of the self-assembled stacked layers, both in PANIs and PANICNs. During intercalation, the PANI-dopant chains get confined between the clay layers and the distance between the clay layers is increased in

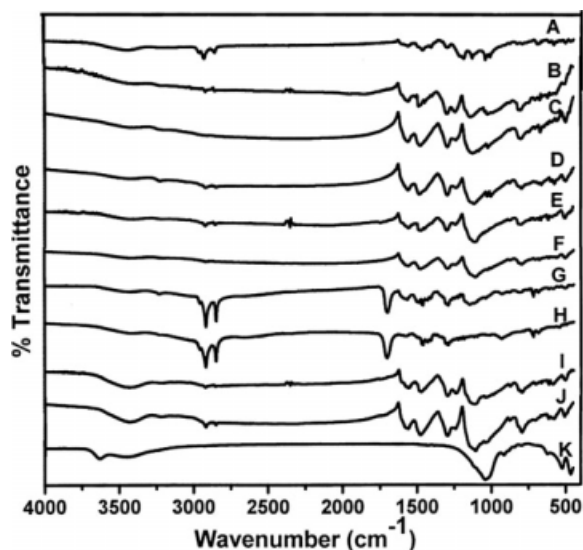
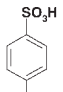
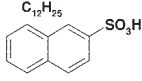
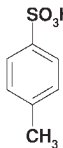

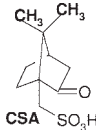
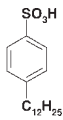
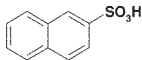
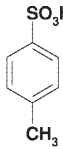

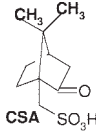


Figure 2 FT-IR spectra of (A) PANI-DBSA, (B) PANI-NSA, (C) PANI-PTSA, (D) PANI-SA, (E) PANI-CSA, (F) PANICN-DBSA, (G) PANICN-NSA, (H) PANICN-PTSA, (I) PANICN-SA, (J) PANICN-CSA, and (K) Na^+ cloisite.

TABLE III
Characterisation of PANIs and PANICNs

Sample	Dopant	XRD studies d spacings (Å)	Dimension of the doped PANI from MMX calculation	Conductivity (S/cm)	Morphology from SEM
PANI-DBSA		29.33, 15	9.8 Å	1.6×10^{-2}	Nano/micro wires
PANI-NSA		No peak	8.9 Å	1.9×10^{-2}	Spongy
PANI-PTSA		10.89	6.5 Å	2.1×10^{-2}	Granular
PANI-SA		36.86, 18.74,	11.4 Å	8.2×10^{-4}	Layered structures
PANI-CSA		No peak	8 Å	1.5×10^{-3}	Sheet like
PANICN-DBSA		34.05, 14.8,	19.4 Å	1.92×10^{-2}	Aggregated layers
PANICN-NSA		No peak	Exfoliated	5.3×10^{-2}	Nano/micro granules
PANICN-PTSA		14.11, 10.59	16.3 Å	7.5×10^{-2}	Well-defined nano/microrods
PANICN-SA		36.7, 26.65	21 Å	8×10^{-3}	Cluster of nanotubes
PANICN-CSA		16.18	17.6 Å	1.76×10^{-2}	Rice-grain structures

various ways depending on the dimension of the doped PANI chains, layer charge density, and the functionality of the intercalating chains.^{49,38} The dimensions of the both doped PANI and the intercalated PANI in PANICNs were correlated with the dimension calculated using energy minimization MMX programme⁵⁰ and are depicted in Table III. XRD patterns of clay, PANICN-DBSA, PANICN-NSA, PANICN-PTSA, PANICN-SA, and PANICN-CSA are shown in Figure 3(A–E). The d spacing in the direction of d_{001} plane of clay showed diffraction peak at $2\theta = 7.26^\circ$ corresponding to the interlayer

spacing of 12.1 Å. PANICN-DBSA showed reflections at $2\theta = 2.59^\circ$ (d spacing 34 Å) and 5.96° (d spacing 14.8 Å). The d spacing of 34 Å can be ascribed as the thickness of the modified self-assembled PANI-DBSA present in PANICN-DBSA.³⁵ The second reflection corresponds to the displaced d_{001} plane of the clay layer. The enhancement in the interlayer spacing (~ 5.2 Å) observed is very close to the dimension of PANI-DBSA layer lying parallel to the plane of the clay surface.⁵¹ This value is calculated based on the thickness of the corresponding anhydrous aluminum silicate framework (9.6 Å).

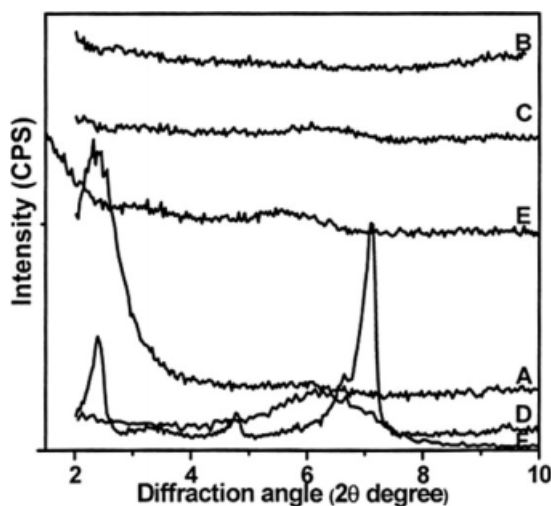


Figure 3 XRD pattern of (A) PANICN-DBSA, (B) PANICN-NSA, (C) PANICN-PTSA, (D) PANICN-SA, (E) PANICN-CSA, and F- Na^+ cloisite.

This result is reminiscent with the observation made by other researchers using layered materials like V_2O_5 ⁵² and FeOCl .⁵³ In PANICN-PTSA, the reflection is observed at $2\theta = 6.25^\circ$ (d spacing 14.1 Å) and $2\theta = 8.34^\circ$ (d spacing 10.59 Å). This increase in dimension of 4.5 Å corresponds to the dimension of the protonated PANI-PTSA. PANICN-SA exhibited diffraction peaks at $2\theta = 2.4^\circ$ (d spacing 36.7 Å), $2\theta = 3.3^\circ$ (d spacing 26.6 Å), $2\theta = 4.77^\circ$ (d spacing 18.5 Å). The initial reflection corresponds to the dimension of the electrostatically self-assembled PANI-SA layers over the nanoclay layers. Here, the characteristic peak of d_{001} plane of the clay is shifted to 26.65 Å corresponding to the dimension of PANI-SA (14.4 Å) in PANICN-SA. The diffractogram of PANICN-NSA did not exhibit any peak corresponding to the d_{001} plane of clay, revealing highly exfoliated clay layers in PANICN-NSA. PANICN-CSA exhibited reflection around $2\theta = 5.45^\circ$ (d spacing 16.18 Å) corresponding to the dimension of the confined PANI-CSA in PANICN-CSA.

Diffractogram of PANI-DBSA, PANI-NSA, PANI-PTSA, PANI-SA, and PANI-CSA are as shown in Figure 4(A–E). PANI-DBSA showed peak at 29.3 Å corresponding to the thickness of the aggregates formed by the electrostatic layer-by-layer self-assembled structure as reported by Taka et al.⁵⁴ The diffractogram of PANI-NSA and PANI-CSA exhibited silent peak revealing the formation of nonoriented structures. PANI-PTSA showed peak at 10.89 Å and this value is agreeing with the dimension of the repeating length of the ordered structure of PANI-PTSA as calculated using energy minimization MMX programme. The diffractogram of PANI-SA exhibited reflection at 36.9, 18.7, 13.6, 12.6, and 9.6 Å indicating the formation of self-assembled aggregates

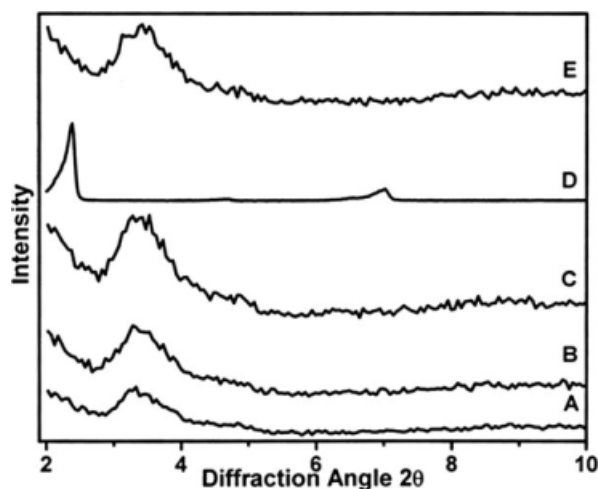


Figure 4 XRD pattern of (A) PANI-DBSA, (B) PANI-NSA, (C) PANI-PTSA, (D) PANI-SA, and (E) PANI-CSA.

of PANI-SA. Similar XRD results were reported for SA (ICDD pattern 381,923) with 001 peak of 39.62 Å positioned approximately at $2\theta = 2.2^\circ$. The energy-minimized structures with dimension of PANI-DBSA, PANI-NSA, PANI-PTSA, PANI-SA, and PANI-CSA calculated using MMX programme are shown in Figure 5(A–E). The difference in the calculated value and the value observed from XRD measurement are due to the conformational changes in the doped PANIs affected by the combination of the various noncovalent interactions during the formation of self-assembled aggregates and also conformational change occurring during the confinement of the PANI chains in the constrained environment. It may be interesting to note that in all cases, the characteristic d_{001} values of PANIs, vanished in PANICNs and new peaks

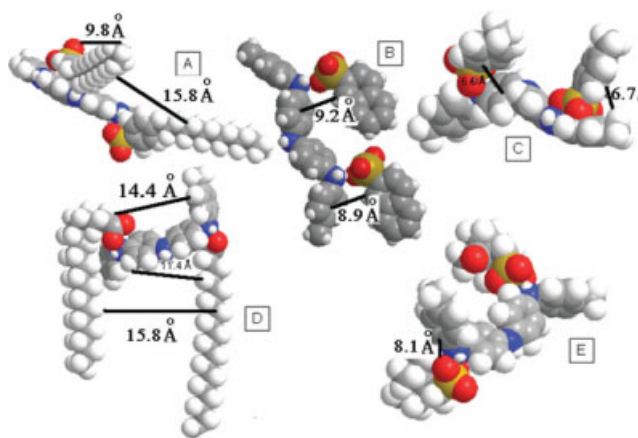


Figure 5 Energy minimization models of (A) PANI-DBSA, (B) PANI-NSA, (C) PANI-PTSA, (D) PANI-SA, and (E) PANI-CSA. [Color figure can be viewed in the online issue, which is available at www.interscience.wiley.com.]

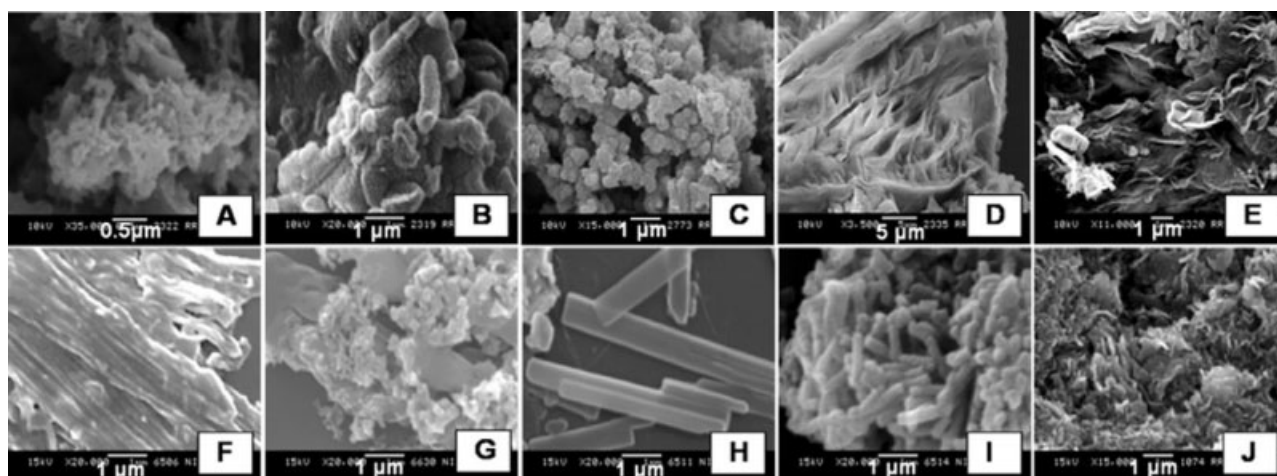


Figure 6 SEM pictures of (A) PANI-DBSA, (B) PANI-NSA, (C) PANI-PTSA, (D) PANI-SA, (E) PANI-CSA, (F) PANICN-DBSA, (G) PANICN-NSA, (H) PANICN-PTSA, (I) PANICN-SA, and (J) PANICN-CSA.

appeared with a higher d spacing, indicating the formation of the modified layered structures of protonated PANIs engulfed on clay surface. Similar studies on the interaction of alkyl chain having polar head group of the organic molecule with the clay surface which form self-assembled structure on the clay surface was reported earlier by Brindley and Moll.⁵⁵

Morphology

Morphology of PANIs and PANICNs was studied using scanning electron microscopy with pelletized samples and the details of the observed morphology are tabulated in Table III. The microstructure of PANICNs is observed to be highly dependent on the functionality of the amphiphilic dopant. The micrograph of PANI-DBSA, PANI-NSA, PANI-PTSA, PANI-SA, PANI-CSA, PANICN-DBSA, PANICN-NSA, PANICN-PTSA, PANICN-SA, and PANICN-CSA are shown in Figure 6(A–J). PANI-DBSA showed nano/micro wires of ~ 100 nm size [Fig. 6(A)]. Spongy core-like structures with a size of 250 nm is observed for PANI-NSA [Fig. 6(B)]. Micrographs of PANI-PTSA exhibited 200 to 300 nm sized clusters of spherical particles [Fig. 6(C)]. PANI-SA showed layered structures having dimension of 500 nm [Fig. 6(D)] and the morphology of PANI-CSA exhibited sheet with thickness ~ 100 nm [Fig. 6(E)].

During intercalation, the morphology of PANIs in the nanocomposites changed due to the presence of clays. PANICN-DBSA exhibited aggregated layers having thickness of 250 to 500 nm [Fig. 6(F)], whereas PANICN-NSA was observed as 100 nm sized granules [Fig. 6(G)]. The micrographs of PANICN-PTSA exhibited well-defined rods having thickness of ~ 200 nm and length of 6 to 7 μm [Fig. 6(H)]. PANICN-SA showed clusters of ~ 100 nm thickness

and 1 μm length [Fig. 6(I)]. The micrographs of PANICN-CSA exhibited rice-grain structures with ~ 150 nm size [Fig. 6(J)]. The various morphology observed in protonated PANIs and PANICNs can be ascribed due to the formation of various modes of self-assembling arising from the combined effect of noncovalent interaction among the PANI chains, dopant–PANI interaction and also different extent of ion–dipole interactions between the clay and protonated PANIs and also due to the electrostatic layer-by-layer stacking.

Thermal properties

Thermal stabilities of PANIs and PANICNs were studied by thermogravimetric analysis at a heating rate of $10^\circ\text{C}/\text{min}$ in nitrogen atmosphere. Thermograms of doped PANIs and PANICNs are shown in Figures 7(A–E) and 8(A–E), respectively.

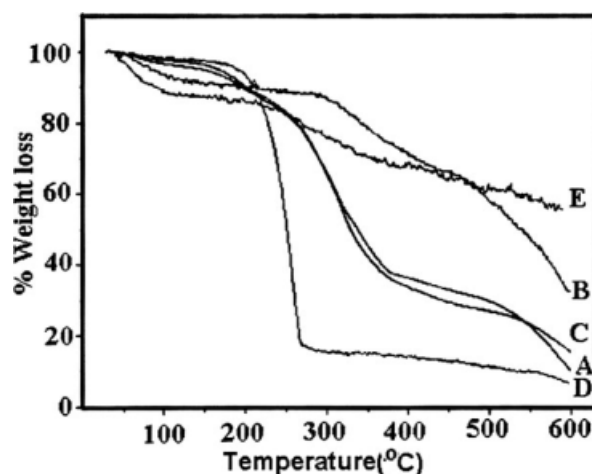


Figure 7 TGA plot of (A) PANI-DBSA, (B) PANI-NSA, (C) PANI-PTSA, (D) PANI-SA, and (E) PANI-CSA.

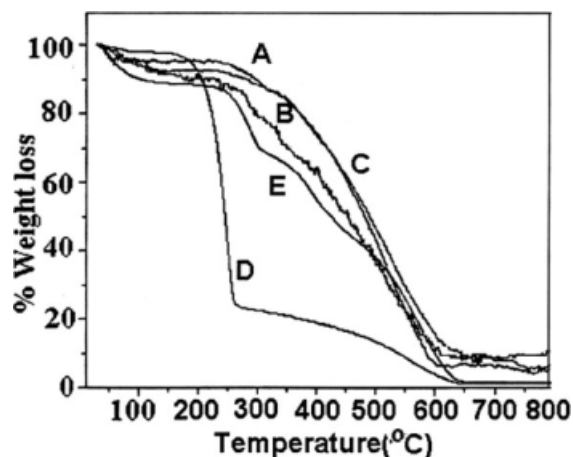


Figure 8 TGA plot of (A) PANICN-DBSA, (B) PANICN-NSA, (C) PANICN-PTSA, (D) PANICN-SA, and (E) PANICN-CSA.

Generally, all PANIs and PANICNs exhibited two-stage decomposition pattern. The weight loss observed below 100°C can be considered due to the removal of absorbed moisture and low-molecular weight volatile compounds present in the protonated PANIs. The second-stage weight loss can be due to decomposition of the amphiphilic dopant molecule present in the doped PANI. Details of the thermal decomposition temperature of PANIs and PANICNs are given in Table IV. Thermal stability of PANIs is in the order PANI-PTSA > PANI-NSA > PANI-CSA > PANI-DBSA > PANI-SA. It can be observed that PANICN exhibited higher maximum decomposition temperature than the corresponding PANIs. Thermal stability of PANICNs also followed the order PANICN-PTSA > PANICN-NSA > PANICN-CSA > PANICN-DBSA > PANICN-SA. The higher thermal stability observed for PANICNs, compared with PANIs, is due to the presence of insulative nanoclay layers.

Thermal phase transition temperatures of PANIs and PANICNs were studied by DSC at a heating rate of 10°C/min in nitrogen atmosphere. Details of thermal transition temperatures of PANIs and PAN-

ICNs are given in Table IV. On heating, PANICNs undergo change in energy that can be attributed from two factors. First transition is arising from the conformational change due to the loss of intermolecular hydrogen-bonded interaction between the protonated PANI chains.⁵⁶ It can also be considered as arising from the crystallization melting temperature of self-assembled protonated PANIs. The phase transition might be due to the guest–host interaction between protonated PANI chains and the clay layer. These observations were further strengthened by the studies made by FT-IR spectroscopy. Phase-transition temperature of PANIs observed to be in the order PANI-SA (56°C) < PANI-DBSA (109°C) ~ PANI-PTSA (109°C) < PANI-NSA (110°C) < PANI-CSA (122°C) and for PANICNs, the phase-transition temperature order is PANICN-NSA (119°C) < PANICN-DBSA (120°C) < PANICN-PTSA (122°C) < PANICN-SA (136.53°C) < PANICN-CSA (136.2°C). Generally, a higher phase-transition temperature was observed for PANICNs compared with PANIs due to the presence of nanoclay layers.

Electrical properties

Electrical conductivity (σ_{dc}) measurements of PANIs and PANICNs using different dopants are illustrated in Table III. PANIs exhibited conductivity in the order of PANI-PTSA (2.1×10^{-2} S/cm) > PANI-NSA (1.9×10^{-2} S/cm) > PANI-DBSA (1.6×10^{-2} S/cm) > PANI-CSA (1.5×10^{-3} S/cm) > PANI-SA (8.2×10^{-4} S/cm). PANICNs also showed the same trends in the order of conductivity as shown by PANIs. The measured conductivity values for PANICNs are PANICN-PTSA (7.5×10^{-2} S/cm) > PANICN-NSA (5.3×10^{-2} S/cm) > PANICN-DBSA (1.92×10^{-2} S/cm) > PANICN-CSA (1.76×10^{-2} S/cm) > PANICN-SA (8×10^{-3} S/cm). Although the order for both PANIs and PANICNs were similar, the conductivity values are greater for PANICNs, e.g., PANICN-PTSA (7.5×10^{-2} S/cm) > PANI-PTSA (2.1×10^{-2} S/cm). Measurement showed that conductivity varied with the change in the functionality of the

TABLE IV
Thermal Stability Studies of PANIs and PANICNs

Sample	PANIs				PANICNs				
	Weight loss up to 100°C (%)	T_{max}	% Weight loss at T_{max}	Phase transition temperature (°C)	Sample	Weight loss up to 100°C (%)	T_{max}	% Weight loss at T_{max}	Phase transition temperature (°C)
PANI-DBSA	3.1	301	36	109.9	PANICN-DBSA	10.42	421	34	120.8
PANI-NSA	6.3	347	20	110	PANICN-NSA	4.89	482	50	119.8
PANI-PTSA	3	484	60	109	PANICN-PTSA	5.81	517	52	122.8
PANI-SA	1.18	250	50	56	PANICN-SA	1.65	266	70	136.5
PANI-CSA	11	314	25	122	PANICN-CSA	5.8	455	52	136.2

dopants. Literature revealed that the conductivity is controlled by two factors.⁵⁷ In one hand, when the content of PANI is very low compared with clay, the insulative clay will affect the effective electron/polaron transfer mechanism and will exhibit low conductivity. At higher concentration of PANI, the insulative clay interlayer disrupts the three-dimensional organization of PANI chains and will therefore lead to an expanded conformation for PANI chains in the confined environment. The polarons and bipolarons will be in the delocalized state and will exhibit higher conductivity for PANICNs than PANIs. These observations were further strengthened by the studies made by UV-vis spectroscopy. UV-vis spectra of PANICNs showed a red shift for the peak corresponding to the transition to the polaron band, consequently the band gap is reduced. Thus, the electrical conductivity is influenced by the size, functionality, and amount of the doped PANI chains present in the system.

CONCLUSIONS

We could successfully synthesize electrically conductive micro/nanostructured PANI and PANICN using five different amphiphilic dopants built with backbone naphthyl, alicyclic, alkyl, and phenyl group by in-situ intercalative emulsion polymerization at room temperature. Studies on UV-vis spectra, FT-IR spectra, XRD, SEM, electrical conductivity, and thermal studies revealed that the rigidity and functionality of the dopant has got profound influence on the electrical conductivity, morphology, thermal stability, and phase transition temperature of PANIs and PANICNs. The variations in the morphology and the electrical conductivity of PANIs and PANICNs are due to the change in the modes of self-assembling arising from the combination of various noncovalent interactions like intermolecular hydrogen bonding, ion-dipole interaction, electrostatic layer-by-layer stacking, and interplane phenyl-phenyl stacking among the PANI chains, PANI-dopant, and PANI clay surfaces. Thermal stability and phase-transition temperature of PANICNs were observed to be higher than doped PANIs due to the presence of nanoclay layers in the former.

We thank Council of Scientific and Industrial Research, India for their financial support from Senior research fellowship and also Indian Space Research Organisation for their financial support from project GAP 109439. We also thank Dr. P. Prabhakar Rao, Dr. C.H. Suresh, Mr. Chandran, and Mr. P.Guruswamy for all their useful discussions and analytical support.

References

1. Yeh, J. M.; Liou, S. J.; Lai, C. Y.; Wu, P. C. *Chem Mater* 2001, 13, 1131.
2. Do Nascimento, G. M.; Constantino, V. R. L.; Temperini, M. L. A. *Macromolecules* 2002, 35, 7535.
3. Goddard, Y. A.; Vold, R. L.; Hoatson, G. L. *Macromolecules* 2003, 36, 1162.
4. Kim, B. H.; Jung, J. H.; Hong, S. H.; Joo, J.; Epstein, A. J.; Mizoguchi, K.; Kim, J. W.; Choi, H. J. *Macromolecules* 2002, 35, 1419.
5. Do Nascimento, G. M.; Constantino, V. R. L.; Landers, R.; Temperini, M. L. A. *Macromolecules* 2004, 37, 9373.
6. Bae, W. J.; Kim, K. H.; Jo, W. H.; Park, Y. H. *Macromolecules* 2004, 37, 9850.
7. Liu, Y. C.; Tsai, C. J. *Chem Mater* 2003, 15, 320.
8. Kuila, B. K.; Nandi, A. K. *Macromolecules* 2004, 37, 8577.
9. Kuila, B. K.; Nandi, A. K. *Macromolecules* 2006, 39, 1621.
10. Caja, J.; Kaner, R. B.; Macdiarmid, A. G. *J Electrochem Soc* 1984, 131, 2744.
11. Abdelaziz, R.; Yang, D. *J Mater Lett* 2008, 62, 4311.
12. Chen, H.; Chen, J.; Aoki, K.; Nishiumi, T. *Electrochim Acta* 2008, 53, 7100.
13. Hong, S. F.; Hwang, S. C.; Chen, L. C. *Electrochim Acta* 2008, 53, 6215.
14. Hirao, T. *Coord Chem Rev* 2002, 226, 81.
15. Deore, B. A.; Yu, I.; Freund, M. S. *J Am Chem Soc* 2004, 126, 52.
16. Huang, J.; Wan, M. *Desalination* 1999, 37, 151.
17. Gupta, Y.; Wakeman, R.; Klaus, H. *J Polym Sci A Polym Chem* 2006, 44, 474.
18. Martin, C. R. *Science* 1994, 266, 1961.
19. Xiong, S.; Wang, Q.; Xia, H. *Synth Met* 2004, 146, 37.
20. Sudha, J. D.; Reena, V. L.; Pavithran, C. *J Polym Sci B Polym Phys* 2007, 45, 2664.
21. Sudha, J. D.; Reena, V. L. *Macromol Symp* 2007, 254, 274.
22. Han, M. G.; Cho, S. K.; Oh, S. G.; Im, S. S. *Synth Met* 2002, 126, 53.
23. Haung, J.; Kaner, R. B. *J Am Chem Soc* 2004, 126, 851.
24. Martin, C. R. *Chem Mater* 1996, 8, 1739.
25. Martin, C. R. *Acc Chem Res* 1995, 28, 61.
26. Kerr, T. A.; Wu, H.; Nazar, L. F. *Chem Mater* 1996, 8, 2005.
27. Lan, T. T.; Pinnavaia, J. *Chem Mater* 1994, 6, 2216.
28. Adams, P. N.; Devasagayam, P.; Pomfret, S. J.; Abell, L.; Monkman, A. *J Phys Condens Matter* 1998, 10, 8293.
29. Kim, B. H.; Jung, J. H.; Kim, J. W.; Choi, H. J.; Joo, J. *Synth Met* 2001, 117, 115.
30. Kim, B. H.; Jung, J. H.; Kim, J. W.; Choi, H. J.; Joo, J. *Synth Met* 2001, 121, 1311.
31. Kim, J. W.; Choi, H. J.; John, M. S. *Makromol Rapid Commun* 1999, 20, 450.
32. Chan, H. S. O.; Nag, S. C.; Ho, P. K. *Macromolecules* 1994, 27, 2159.
33. Laska, J.; Pron, A.; Lefrant, S. *J Polym Sci A Polym Chem* 1995, 33, 1437.
34. Raji, K. P.; Veena, V.; Pillai, C. K. S. *Synth Met* 1999, 104, 189.
35. Jia, W.; Segal, E.; Kornemandel, D.; Lamhot, Y.; Narkis, M.; Siegmann, A. *Synth Met* 2002, 128, 115.
36. Stejskal, J.; Kratochvil, P.; Jankins, A. D. *Polymer* 1996, 37, 367.
37. Wan, M. *J Appl Polym Sci* 2003, 55, 399.
38. Xia, Y.; Wiesinger, J. M.; Macdiarmid, A. G.; Epstein, A. J. *Chem Mater* 1995, 7, 443.
39. Ruokolainen, J.; Eerikainen, H.; Torkkeli, M.; Serimaa, R.; Jusila, M.; Ikkala, O. *Macromolecules* 2000, 33, 9272.
40. Lv, R.; Zhang, S.; Shi, Q.; Kan, J. *Synth Met* 2005, 150, 115.

41. Epstein, A. J.; Ginder, J. M.; Zhuo, F.; Woo, H. S.; Tanner, D. B.; Richter, A. F.; Angelopoulos, M.; Huang, W. S.; Alan, G. M. *Synth Met* 1987, 13, 63.
42. Stubican, V.; Roy, R. *J Am Cer Soc* 1961, 44, 625.
43. Liu, Y. J.; Kanatzidis, M. G. *Inorg Chem* 1993, 32, 2989.
44. Kanatzidis, M. G.; Wu, C. G.; Marcy, H. O.; Degroot, D. C.; Kannewurf, C. R.; Kostikas, A. *Adv Mater* 1990, 2, 364.
45. He, H.; Frost, R. L.; Deng, F.; Zhu, J.; Wen, X.; Yuan, P. *Clays Clay Miner* 2004, 52, 350.
46. Li, X. G.; Lu, Q. F.; Huang, M. R. *Chem A Eur J* 2006, 12, 1349.
47. Alan, G. M.; Arthur, J. E. *Synth Met* 1995, 69, 85.
48. Cao, Y.; Li, S.; Xue, Z.; Guo, D. *Synth Met* 1986, 16, 305.
49. Chen, S. A.; Hwang, G. W. *J Am Chem Soc* 1995, 117, 10055.
50. Gajewski, K. I.; Gilberr, M. H.; Liotta, D. In *Advances in Molecular Modeling*; JAI Press: Greenerick, CT, 1990; Vol. 2.
51. Kim, B. H.; Jung, J. H.; Hong, S. H.; Kim, J. W.; Choi, H. J.; Joo, J. *Curr Appl Phys* 2001, 1, 112.
52. Nakajima, H.; Matsubayashi, G. *J Mater Chem* 1995, 5, 105.
53. Kanatzidis, M. G.; Bissessur, R.; Degroot, D. C.; Schindler, J. L.; Kannewurf, C. R. *Chem Mater* 1993, 5, 595.
54. Taka, T.; Laakso, J.; Levon, K. *Solid State Commun* 1994, 92, 393.
55. Brindley, G. W.; Moll, W. F. *Am Mineral* 1965, 50, 1355.
56. Vaia, R. A.; Teukolsky, R. K.; Giannelis, E. P. *Chem Mater* 1994, 6, 1017.
57. Mehrotra, V.; Giannelis, E. P. *Solid State Commun* 1991, 77, 155.